CHEMISTRY OF MATERIALS

Article

pubs.acs.org/cm

Nanoscale Spin-State Ordering in $LaCoO_3$ Epitaxial Thin Films

Ji-Hwan Kwon,[†,‡,§] Woo Seok Choi,[∥,⊥] Young-Kyun Kwon,[#] Ranju Jung,[▽] Jian-Min Zuo,[§] Ho Nyung Lee,[∥] and Miyoung Kim*[,†,‡]

[†]Center for Correlated Electron Systems, Institute for Basic Science (IBS), Seoul 151-747, Republic of Korea

[‡]Department of Materials Science and Engineering and Research Institute of Advanced Materials, Seoul National University, Seoul 151-744, Republic of Korea

[§]Department of Materials Science and Engineering and Frederick Seitz Materials Research Laboratory, University of Illinois at Urbana−Champaign Urbana, Illinois 61801, United States

[∥]Materials Science and Technology Division, Oak Ridge National Laboratory Oak Ridge, Tennessee 37831, United States

[⊥]Department of Physics, Sungkyunkwan University Suwon 440-746, Republic of Korea

[#]Department of Physics and Research Institute for Basic Sciences, Kyung Hee University Seoul 130-701, Republic of Korea

[▽]Department of Electrophysics, Kwangwoon University Seoul 139-701, Republic of Korea

Supporting Information

ABSTRACT: The nature of magnetic ordering in $LaCoO_3$ epitaxial thin films has been the subject of considerable debate. We present direct observations of the spin-state modulation of Co ions in $LaCoO_3$ epitaxial thin films on an atomic scale using aberration-corrected scanning transmission electron microscopy (STEM), electron energy loss spectroscopy (EELS), and *ab initio* calculations based on density functional theory (DFT) calculations. The results of an atomic-resolution STEM/EELS study indicate that the superstructure is not associated with oxygen vacancies; rather, it is associated with a higher spin state of Co^{3+} ions and their ordering. DFT calculations successfully reproduced the modulation of lattice spacing with the introduction of spin ordering. This result identifies the origins of intrinsic phenomena in strained $LaCoO_3$ and provides fundamental clues for understanding ferromagnetism in Co-based oxides.

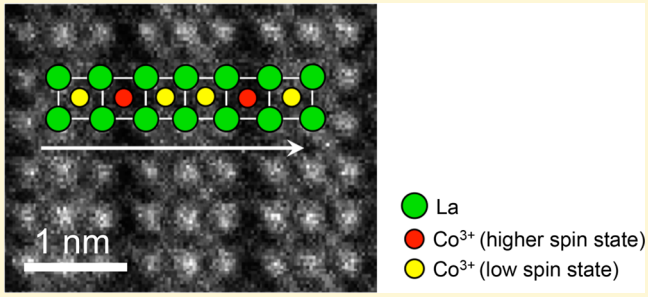

1. INTRODUCTION

Perovskite cobaltites have attracted considerable attention due to their useful magnetic and associated transport properties. Their intriguing physical properties, which are attributed to various spin states of cobalt ions determined by the delicate competition between crystal field splitting and Hund's exchange energy,[1] provide great potential for new functional applications in electronics and spintronics. The multivalency of Co ion is also useful for an extensive range of technological applications, including cathodes in solid-oxide fuel cells and batteries[2,3] and oxygen-permeable membranes.[4]

Among all perovskite-type cobaltites, lanthanum cobaltite ($LaCoO_3$, LCO) provides an interesting foundation for studying the spin-state transition and related phenomena. LCO exhibits a stable $3d^6$ valence state and a rhombohedral structure (a = 5.38 Å, β = 60.81°, and pseudocubic a_0 = 3.80 Å);[5] it exhibits three spin states: low spin (LS), intermediate spin (IS), and high spin (HS). At low temperatures (T < 35 K), bulk LCO exhibits a nonmagnetic ground state with a LS state for the Co^{3+} ions (S = 0, $t_{2g}^6e_g^0$). As the temperature increases, a spin-state transition from LS to IS (S = 1, $t_{2g}^5e_g^1$) and/or HS (S = 2, $t_{2g}^4e_g^2$) occurs. In addition to temperature, external pressure or doping also influences the spin states.[6,7] Numerous experimental and theoretical studies on the nature of the spin-state transition have been conducted. Some studies have suggested a first-order transition from a LS state to a HS state,[8,9] whereas other studies invoked the IS state.[10,12,13] In contrast to bulk LCO, LCO epitaxial thin films exhibited robust ferromagnetic ordering at temperatures less than ∼80 K.[14,15] Various mechanisms, including the strain-induced transformation of atomic configurations (either through lattice expansion or rotation of the Co−O octahedra), double exchange by oxygen nonstoichiometry, and the effects of Co ions on the surface of thin films, have been proposed to account for the origin of ferromagnetic ordering.[14−19] However, the exact microscopic origin of the ferromagnetic state and spin-state transition remained unclear.

Certain authors have recently reported an unconventional strain relaxation phenomenon in LCO epitaxial thin films. High quality of epitaxial LCO thin films have been grown on various

Received: October 19, 2013
Revised: March 13, 2014
Published: March 18, 2014

   dx.doi.org/10.1021/cm5003115 | Chem. Mater. 2014, 26, 2496−2501

substrates $LaAlO_3$, $(LaAlO_3)_{0.29}(SrAl_{0.5}Ta_{0.5}O_3)_{0.71}$, and $SrTiO_3$ (STO), exhibiting strain dependent microscopic lattice modulations. Despite the fact that atomically ordered patterns that formed as a consequence of local symmetry change in epitaxial LCO thin films were responsible for ferromagnetic ordering, exact atomic, and electronic structures are still under a veil.[20] In this study, we have studied atomic and electronic structure of LCO epitaxial thin films on STO that shows periodic lattice modulation. By directly probing the different spin states of Co ions with scanning transmission electron microscopy (STEM)−electron energy loss spectroscopy (EELS) on an atomic scale, we investigated the atomistic origin of ferromagnetic ordering in atomically ordered high-quality LCO epitaxial thin films. We performed first-principles calculations based on DFT to unambiguously understand the experimentally observed spin-state ordering.

2. EXPERIMENTAL AND COMPUTATIONAL METHODS

Epitaxial LCO thin films were grown on STO substrates by pulsed laser epitaxy. LCO thin film is subjected to tensile strain (ε = 2.6%) on the STO substrate. Details of the sample synthesis are provided elsewhere.[20]

2.1. Transmission Electron Microscopy. Samples for TEM were prepared by mechanical polishing and ion milling using the procedure previously reported for other oxide thin films. This procedure did not introduce redundant oxygen vacancies.[21] Electron microscopy was performed using JEOL-ARM200F for EELS and Titan^3 G2 60-300 instruments for imaging with a high-angle annular dark field (HAADF) detector with a cutoff angle of 100 mrad. The convergence angle was 30 mrad and collection angle was 60 mrad. An acceleration voltage of 80 kV was used in the atomic-resolution EELS experiments to avoid electron beam damages while EELS experiment. The JEOL-ARM200F was equipped with Cold-FEG and GIF Quantum ER. The energy resolution was measured to be as 0.4 eV at 80 kV. The line scan spectra were acquired with exposure time of 1 s/point, the entrance aperture was 5 mm, and camera length was 2 cm.

2.2. Density Functional Theory Calculations. The projector augmented wave (PAW)[22] method and spin-polarized generalized-gradient approximation (GGA), which is implemented in the VASP code,[23,24] was used in the DFT calculations.[25] The generalized-gradient approximation (GGA) + U method with an effective Hubbard parameter $U_{eff} = U - J$ was used to describe the exchange and correlation. Recent first-principles calculations have shown that the experimentally observed low-spin (S = 0) ground state is only stable for U_{eff} values less than 4 eV.[19] In our calculations, we used U_{eff} = 3 eV, similar to previous studies.[19,26] To induce tensile strain applied by the STO substrate, the in-plane lattice constant was constrained to the theoretical value of 3.95 Å, in which bulk cubic STO exhibits the lowest total energy. The lattice constant along the out-of-plane direction was fixed at a value of 3.77 Å with the lowest total energy, which we systematically determined by varying the lattice constant along the c-axis. Four different spin configurations in the 3 × 1 supercell were considered (Figure 3). (We refer to the higher-spin state (i.e. S > 0) of the Co^{3+} ion as 'H' and to the low-spin state as 'L'.) The atomic relaxations were terminated when the interatomic forces were less than 0.02 eV/Å.

3. RESULTS

3.1. Microstructure of $LaCoO_3$ Thin Films. Figure 1a shows a cross-sectional image from high-angle annular dark field (HAADF) STEM of a LCO thin film grown on a (001) $SrTiO_3$ (STO) substrate. A distinct and atomically sharp interface between LCO and STO was observed. Interestingly, we observed well-ordered dark stripes running perpendicular to the LCO/STO interface. The dark stripes appeared as a result of a regular superstructure with a periodicity of $3a_0$ (∼1.2 nm).

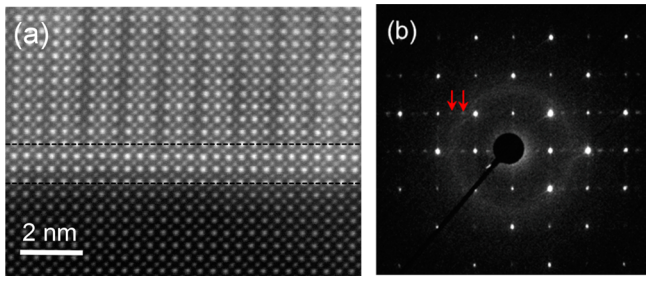

Figure 1. (a) Atomic-resolution HAADF-STEM image of LCO/STO that shows an intriguing pattern of dark stripes. The dark stripes appeared as a regular superstructure with a periodicity of $3a_0$ (∼1.2 nm). (b) Electron diffraction pattern of the LCO thin film. The reflections from the superstructure are denoted by arrows.

A distinct superstructure was observed in the electron diffraction (ED) pattern that was evident in this region of dark stripes, as shown in Figure 1b. The strong reflections in the ED image are associated with a typical perovskite structure, whereas the weak reflections indicated by the arrows originate from the superstructure with a periodicity of $3a_0$. Notably, areas without dark stripes were observed in areas, presumably, in which this pattern of dark stripes propagated along the electron beam direction. Structural dislocations were only observed in the stripe-free domains. We confirmed the assumption that superstructures occur in two dimensions in LCO thin films by examining two TEM specimens that were prepared perpendicular to each other. We believe that the pattern of dark stripes formed as a domain and propagated along the crystallographically equivalent [100] or [010] direction by relaxing in the same manner. Note that the areas of the stripe-free region and the stripe region are comparable each other. The detailed model of this superstructure is included in the Supporting Information. These striped patterns, however, were not observed in the vicinity of the substrate near the first three unit cells (Figure 1a). In this interface region, the La−La interatomic distance was uniform and was similar to the interatomic distance of the Sr−Sr in the STO substrate (∼3.9 Å).[20] This result indicates that the interface region near the first three unit cells is coherently strained to the substrate. Above the first three unit cells, the La−La interatomic distance across the dark stripes was greater than the interatomic distances in the other bright layers. In the STEM imaging, an increased interatomic distance yields a reduced intensity overlap between adjacent atoms, which causes the appearance of a dark striped layer. This contrast modulation has been frequently observed in oxides with ordered oxygen vacancies[27−29] because columns with such vacancies repel each other.

3.2. Electronic Structure of the Striped Pattern in $LaCoO_3$ Thin Films. To elucidate the origins of atomic distance modulation and corresponding magnetic ordering, we examined electronic structures using EELS. We carefully determined whether the striped patterns were associated with the formation of oxygen vacancies because oxygen vacancy ordering, which generates a similar atomic configuration, has been frequently ascribed to the origin of magnetic ordering in other cobaltites.[27,28,30,31] Figure 2a shows an atomic-resolution HAADF image in which an EELS line scan was performed. To improve the signal-to-noise ratio of the EELS data shown in Figures 2b and c, six spectra were integrated in the bright and dark layers. Three characteristic peaks, which are representative features of the bulk perovskite LCO structure, were observed in

dx.doi.org/10.1021/cm5003115 | Chem. Mater. 2014, 26, 2496−2501

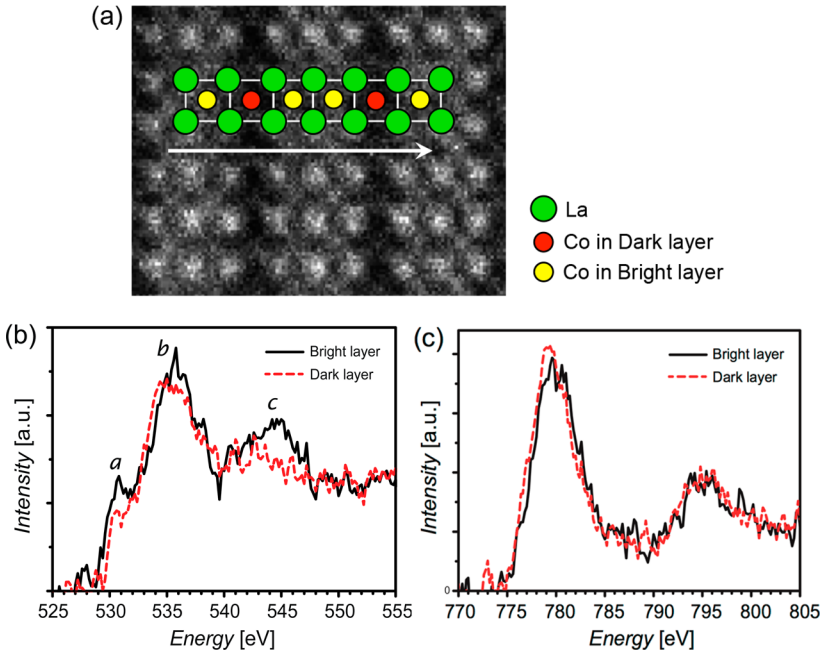

Figure 2. (a) Atomic-resolution HAADF-STEM image in which EEL spectra were acquired across the dark layer, (b) O *K* edges in the bright and dark layers, and (c) Co $L_{2,3}$ edges in the bright and dark layers. The six signals were integrated to improve the signal-to-noise ratio.

the O *K* edge spectrum of our LCO thin film (Figure 2b).[11,13] The prepeak, which is labeled *a*, can be assigned to the hybridization of O 2*p* with Co 3*d*, whereas peaks *b* and *c* originated from the hybridization of O 2*p* with La 5*d* and Co 4*sp*, respectively.[11] Three distinct peaks were visible in the bright layer, whereas the intensity of the prepeak *a* from the dark layer was significantly weaker and appeared as a small shoulder. The reduced prepeak of the O *K* edge in cobaltites can be attributed to the formation of oxygen vacancies[27,28] or to the presence of different spin states.[13]

Oxygen vacancies are typical defects in oxides. Ordering of these vacancies has been reported in numerous oxide systems, including heavily doped cobaltites such as $La_{0.5}Sr_{0.5}CoO_{3-\delta}$.[27,28] Other oxides, including ferrites, manganites, and cuprates, can also exhibit similarly ordered oxygen-deficient structures.[29−36] In general, oxygen vacancies serve as electron donors in transition-metal oxides[37] by transferring electrons to the *d* bands of the transition metals, which results in a change in the valence states of the transition metals. In $LaCoO_{3-\delta}$, these transferred electrons caused by oxygen vacancies fill the unoccupied density of states of Co 3*d* hybridized with O 2*p* and cause a reduction in the intensity of the prepeak of the O *K* edge.[27] In addition, transferred electrons that fill the Co 3*d* states change the valence state of Co ions from Co^{3+} to Co^{2+} (high spin), which plays a critical role in the magnetic ordering of cobaltites such as $La_2Co_2O_5$ and $La_3Co_3O_8$.[30,31]

Although the origin of the dark stripes in our LCO films may be due to oxygen vacancies, if only the images and the prepeak of the O *K* edges are considered, the Co *L* near-edge structure, which is sensitive to the valence state of the Co atom,[11,38−40] showed no significant change between the bright and dark layers (Figure 2c). In addition, the L_3/L_2 ratio was almost identical in the dark and bright layers. These findings indicate that the oxidation state of Co remained unchanged throughout the film, which suggests that the film is stoichiometric (see Supporting Information). Previous reports have argued that the Co *L* edge may not change in the presence of oxygen vacancies.[27,28] However, this condition is only valid for the metallic electronic structure of the $La_{0.5}Sr_{0.5}CoO_{3-\delta}$ system.[27,28] Similar to the results of previous studies, the LCO thin films in this study were highly insulating films,[18] and the Co *L* edge was strongly correlated with the local Co valence state. As previously reported, other macroscopic analyses of the sample, such as X-ray absorption spectroscopy (XAS) and spectroscopic ellipsometry, indicated that our LCO thin films were not influenced by oxygen vacancies or other Co-based impurities; that is, the films were stoichiometric.[20]

3.3. Spin-State Ordering in $LaCoO_3$ Thin Films. We considered a modification of the spin-state configuration to explain the origin of the reduced O *K* edge prepeak intensity. According to Klie et al.,[13] the intensity of the O *K* edge prepeak can be used as a direct measure of the spin state in stoichiometric LCO. When Co^{3+} is in a low-spin state, the O *K* edge prepeak is primarily attributed to the Co e_g state. However, as a higher spin state of the Co^{3+} ion emerges, the e_g states are increasingly occupied, which interrupts the charge transfer and decreases the intensity of the O *K* edge prepeak. Our EELS results (Figure 2b) can also be explained by the simulation provided by Klie et al. In our experiment with EELS, the t_{2g} contribution was not evident, which may be attributed to two reasons; first, the π-like Co t_{2g} states would hybridize less strongly with O 2*p* states than Co σ-like e_g states, thus t_{2g} contribution is hard to be observed. Second, the bond length between Co and O increases near the dark layer, resulting in decreased hybridization. Similarly decreased hybridization between O 2*p* and Co 4*s*/4*p* would also explain the reduced intensity of peak *c* in the dark layer in Figure 2b. (EELS simulation based on DFT calculation is included in Supporting Information.) As our LCO was stoichiometric, we can conclude that the decreased intensity of the O *K* edge prepeak results from a higher spin state of Co ions in the dark layers.

The spin-state ordering associated with the atomic-spacing modulation was studied and confirmed using DFT calculations. The total energies of the four different spin configurations are

dx.doi.org/10.1021/cm5003115 | *Chem. Mater.* 2014, 26, 2496−2501

summarized in Table 1. The total energy of LLL was used as a reference. The HLL configuration was the most stable

Table 1. Total Energies and Magnetic Moments of Four Different Spin Configurations of Co^{3+} Ions

spin configurations	HHH	HHL	HLL	LLL
energy [eV]	−0.25	−0.34	−0.41	0
magnetic moment [μ_B/Co]	2.45	2.63	2.75	

configuration among the four different configurations, which is consistent with our experimental findings. Interestingly, the relaxed atomic structure of HLL also reproduced the experimentally observed structure, which comprises a larger La−La interatomic distance in the higher-spin states (4.17 Å) than in the other two layers (3.83 Å) for every three unit cells (Figure 3c). Larger interatomic distances of higher-spin states are ascribed to the increased ionic radius of the Co^{3+} ion and the equivalently increased Co−O distance, which reduces crystal field splitting.[41] This result is also consistent with the previous result, where the tensile strain was found to stabilize the higher-spin states of Co^{3+} in LCO.[14,20] We also found a larger interatomic distance for the H layer in the HHL structure; however, the difference between the interatomic distances was smaller than the difference between the interatomic distances in the HLL structure. Moreover, the HHL structure should exhibit bright stripes (dark−dark−bright) instead of dark stripes in the STEM image, which was not observed in our LCO thin films. The atomic distances in the HHH and LLL structures were equivalent to the initial values. Therefore, the DFT results successfully reproduced the modulation of the lattice spacing along the in-plane direction by introducing spin-state ordering (higher spin−low spin−low spin), as shown in Figure 1.

The detailed spin configuration of HLL LCO is evidenced by the density of states (DOS). Figure 4, a and b, shows the partial DOS (or PDOS) of a Co atom in the H and L layers, respectively, and Figure 4, c and d, shows the layer DOS (or LDOS) of a CoO_2 layer in the H and L layers, respectively. As shown in Figure 4a, the Co t_{2g} states are completely filled and the Co e_g states are empty, which represents a typical PDOS shape for the LS state of Co in LCO. This result indicates that the Co in the L layer is LS.[42] Conversely, the shape of the DOS in the H layer is distinct from the shape of the DOS in the L layer. The Co e_g states become delocalized near E_F with a strong hybridization of the O 2p states; this behavior is similar to the DOS of the IS Co ions.[19,42] The DOS of the H layer shows metallic features, which is inconsistent with the experimental results but is commonly observed in most theoretical studies.[19,42,43] Previous studies speculated that additional dynamic Jahn−Teller distortion and/or orbital ordering should be considered to explain the insulating behavior of LCO.[19,44] The magnetic moment of Co ion in the H layer, which is dependent on the spin configurations, is calculated as 2.45−2.75 μ_B (Table 1). These values are between the values of intermediate spin states and the values of high-spin states (IS: 2.11 μ_B. HS: 3.16 μ_B) of the cobalt ions.[44] Notably, the HS and IS states of Co reproduced the modulation of the lattice spacing, and the calculation with octahedral tilts/rotations showed similar lattice expansion in the higher-spin state.

4. DISCUSSION

Striped patterns have been interpreted as ordered oxygen vacancies in numerous oxide systems, including Sr-doped and oxygen-deficient $LaCoO_{3-\delta}$.[27,28] However, we have presented evidence that patterns of dark stripes in LCO thin films are most likely not caused by oxygen vacancies. The oxygen vacancy model does not adequately explain the experimental results of microscopic analyses and macroscopic analyses. For example, if the striped patterns originated from oxygen vacancies, a high-density striped pattern implies a high concentration of oxygen deficiencies, which should be easily detected by XAS; approximately 11% oxygen deficiency is expected if we assume that the dark stripes exist in all three unit cells of the superstructure throughout an entire $LaCoO_3$ thin film. However, XAS demonstrates that the LCO thin films are stoichiometric and that the total signal of Co^{2+} is less than 5%, which corresponds to 0.8% oxygen vacancies (Supporting Information). This oxygen deficiency can result in a region of dark stripes that comprises a maximum of ∼7% of the total area

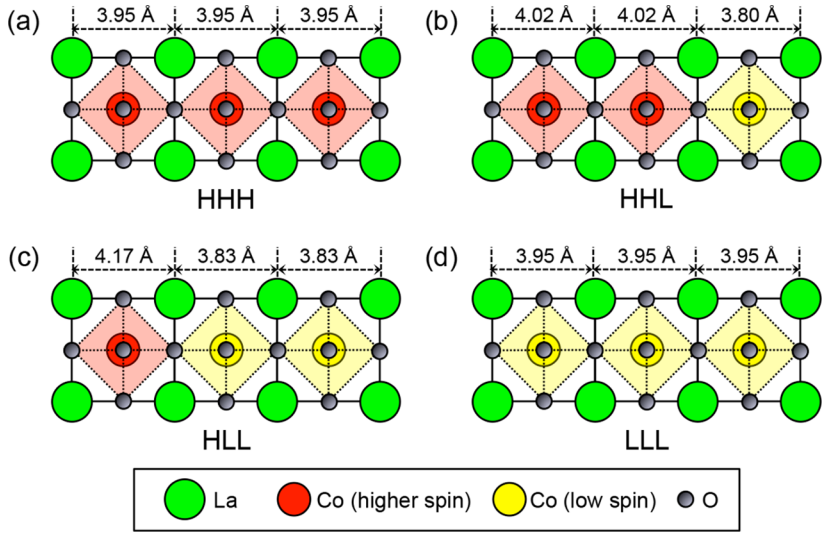

Figure 3. Schematic drawings of four different spin configurations of the 3 × 1 supercell of LCO: (a) HHH, (b) HHL, (c) HLL, and (d) LLL (H: higher-spin state ($S > 0$). L: low-spin state). The La−La interatomic distances are shown.

dx.doi.org/10.1021/cm5003115 | Chem. Mater. 2014, 26, 2496−2501

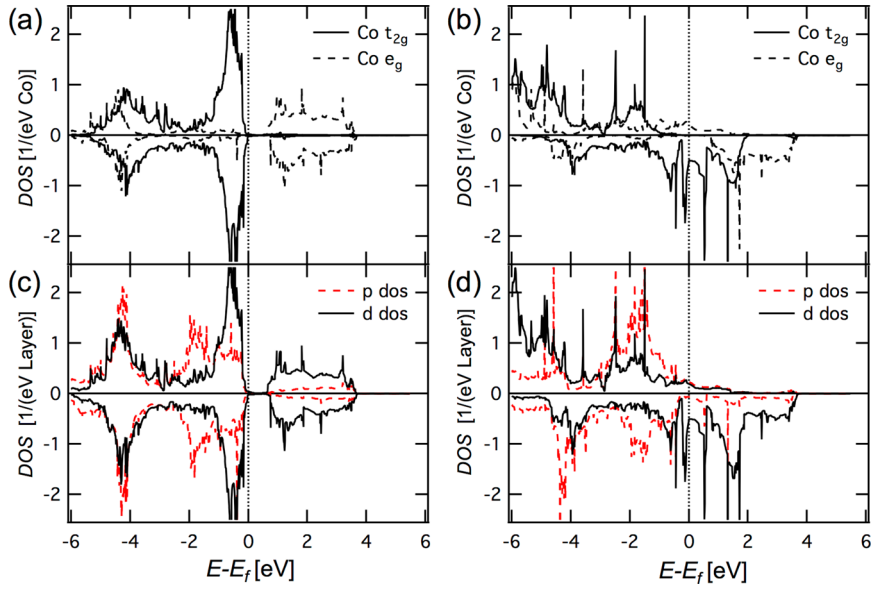

Figure 4. Partial density of states (PDOS) of Co atoms in the (a) L layer and (b) H layer. Layer density of states (LDOS) of the CoO_2 layers in the (c) L layer and (d) H layer.

of the LCO film. However, STEM observations indicate that the majority of areas are covered by the stripes. Despite the possibility that the low concentration of oxygen vacancies is responsible for the stripes, these results indicate that the contribution is minor. In addition, it is worth noting that the optimal growth window for stoichiometric LCO epitaxial thin film is very narrow.[20] Thus, reducing background oxygen pressure for LCO film growth resulted in unwanted impurity phase such as CoO or polycrystalline films rather than creating oxygen vacancies (oxygen-deficient $LaCoO_{3-x}$ thin films), as Co can accommodate different oxidation state readily by the formation of second phases rather than introducing oxygen vacancies. In the EELS analysis, the integrated intensity ratio of Co L_3/L_2 is calculated to be 3.46 ± 0.61 for the bright layer and 3.48 ± 0.48 for the dark layer, which indicates that the local Co valence state does not change throughout the pattern of dark stripes. On the basis of spectroscopic analyses such as XAS, and EELS, we conclude that oxygen vacancies cannot be the main reason for the striped pattern in LCO thin films because the spin-state ordering of Co^{3+} ions contributes to the striped structure in LCO thin films.

The HLL spin configuration persists within a range from 3.78 Å (−2.7%) to 3.98 Å (2.3%) in our calculation. Beyond this range, spin flip occurs and HLL spin ordering cannot be preserved. Note that HLL spin configuration is most stable only in a certain range: tensile strained area from ∼3.88 Å (corresponds to ∼0% strain) to 3.96 Å (corresponds to ∼2.1% tensile strain).

Although the accurate spin state in HLL configuration is highly desirable, we could not determine its *exact* spin state with current DFT results. For LCO thin film, the exact structure is still unclear and we have used a fairly simplified structural model ignoring complex octahedral tilting/rotation and/or Jahn−Teller distortion that could couple with spin configuration, leading more complicated electronic structures.[46] Furthermore, there is a limitation of DFT + U method for describing the complex orbital physics. We believe further theoretical calculations considering more sophisticated method such as dynamic mean-field theory should be performed with more detailed structure for an *exact* spin state of Co ion in the dark layer.[19,45] However, with a simplified atomic structure and DFT + U method, our calculation well reproduces experimentally observed local atomic structures, atomic distance modulations, ascribing to spin ordering of Co ion.

5. CONCLUSIONS

We directly observed spin-state modulation on an atomic scale in strained LCO epitaxial thin films on STO substrates by STEM-EELS, which was complemented by DFT calculations. Atomic-resolution EELS revealed that the lattice-spacing-modulated pattern of dark stripes, which is responsible for ferromagnetic ordering, is not associated with the ordered oxygen vacancy but is associated with the higher spin state of Co^{3+} ions. DFT calculations showed that spin-state ordering, which was stabilized by tensile strain, successfully reproduced the modulation of atomic spacing within nanoscale superstructures by introducing spin-state ordering. These results facilitate a better understanding of ferromagnetism in cobalt-based oxides and form a new approach for investigating interactions between spin, orbital, charge, and lattice degrees of freedom in transition-metal oxides.

■ ASSOCIATED CONTENT

Supporting Information

Spin-ordering model of the $LaCoO_3$ thin film, Determination of stoichiometry of the $LaCoO_3$ thin film (XAS, EELS, DFT), EELS simulation, STEM simulation. This material is available free of charge via the Internet at http://pubs.acs.org.

■ AUTHOR INFORMATION

Corresponding Author

*E-mail: mkim@snu.ac.kr.

Notes

The authors declare no competing financial interest.

■ ACKNOWLEDGMENTS

This work was supported by the National Research Foundation of Korea(NRF) grant funded by the Korea government (MSIP)

(NRF 2013034238 and NRF 2013050169) The work at Oak Ridge National Laboratory was supported by the Basic Energy Sciences, Materials Sciences and Engineering Division of the U.S. Department of Energy. This study was also supported by the National Institute of Supercomputing and Networking/Korea Institute of Science and Technology Information with supercomputing resources and technical support (KSC-2012-C2-088). R. Jung was supported by the research grant of Kwangwoon University in 2014. This work was supported by the Institute for Basic Science (IBS) in Korea.

■ REFERENCES

(1) Raccah, P. M.; Goodenough, J. B. *Phys. Rev.* **1967**, *155*, 932.
(2) Adler, S. B. *Chem. Rev.* **2004**, *104*, 4791−4844.
(3) Poizot, P.; Laruelle, S.; Grugeon, S.; Dupont, L.; Tarascon, J. M. *Nature* **2000**, *407*, 496−499.
(4) Teraoka, Y.; Honbe, Y.; Ishii, J.; Furukawa, H.; Moriguchi, I. *Solid State Ionics* **2002**, *152*, 681−687.
(5) Xu, S.; Moritomo, Y.; Mori, K.; Kamiyama, T.; Saitoh, T.; Nakamura, A. *J. Phys. Soc. Jpn.* **2001**, *70*, 3296.
(6) Mydeen, K.; Mandal, P.; Jin, C. Q.; Prabhakaran, D. *J. Phys.: Conf. Ser.* **2010**, *215*, 012040.
(7) Fuchs, D.; Schweiss, P.; Adelmann, P.; Schwarz, T.; Schneider, R. *Phys. Rev. B* **2005**, *72*, 014466.
(8) Podlesnyak, A.; Streule, S.; Mesot, J.; Medarde, M.; Pomjakushina, E.; Conder, K.; Tanaka, A.; Haverkort, M.; Khomskii, D. *Phys. Rev. Lett.* **2006**, *97*, 247208.
(9) Haverkort, M.; Hu, Z.; Cezar, J.; Burnus, T.; Hartmann, H.; Reuther, M.; Zobel, C.; Lorenz, T.; Tanaka, A.; Brookes, N.; Hsieh, H.; Lin, H. J.; Chen, C.; Tjeng, L. *Phys. Rev. Lett.* **2006**, *97*, 176405.
(10) Saitoh, T.; Mizokawa, T.; Fujimori, A.; Abbate, M.; Takeda, Y.; Takano, M. *Phys. Rev. B* **1997**, *56*, 1290.
(11) Abbate, M.; Fuggle, J. C.; Fujimori, A.; Tjeng, L. H.; Chen, C. T.; Potze, R.; Sawatzky, G. A.; Eisaki, H.; Uchida, S. *Phys. Rev. B* **1993**, *47*, 16124.
(12) Maris, G.; Ren, Y.; Volotchaev, V.; Zobel, C.; Lorenz, T.; Palstra, T. T. M. *Phys. Rev. B* **2003**, *67*, 224423.
(13) Klie, R. F.; Zheng, J. C.; Zhu, Y.; Varela, M.; Wu, J.; Leighton, C. *Phys. Rev. Lett.* **2007**, *99*, 047203.
(14) Fuchs, D.; Pinta, C.; Schwarz, T.; Schweiss, P.; Nagel, P.; Schuppler, S.; Schneider, R.; Merz, M.; G, R.; von Löhneysen, H. *Phys. Rev. B* **2007**, *75*, 144402.
(15) Fuchs, D.; Arac, E.; Pinta, C.; Schuppler, S.; Schneider, R.; von Löhneysen, H. *Phys. Rev. B* **2008**, *77*, 014434.
(16) Yan, J. Q.; Zhou, J. S.; Goodenough, J. B. *Phys. Rev. B* **2004**, *70*, 014402.
(17) Senarıs-Rodrıguez, M. A.; Goodenough, J. B. *J. Solid State Chem.* **1995**, *118*, 323−336.
(18) Freeland, J. W.; Ma, J. X.; Shi, J. *Appl. Phys. Lett.* **2008**, *93*, 212501.
(19) Rondinelli, J.; Spaldin, N. *Phys. Rev. B* **2009**, *79*, 054409.
(20) Choi, W. S.; Kwon, J.-H.; Jeen, H.; Hamann-Borrero, J. E.; Radi, A.; Macke, S.; Sutarto, R.; He, F.; Sawatzky, G. A.; Hinkov, V.; Kim, M.; Lee, H. N. *Nano Lett.* **2012**, *12*, 4966−4970.
(21) Shah, A. B.; Ramasse, Q. M.; Zhai, X.; Wen, J. G.; May, S. J.; Petrov, I.; Bhattacharya, A.; Abbamonte, P.; Eckstein, J. N.; Zuo, J.-M. *Adv. Mater.* **2010**, *22*, 1156−1160.
(22) Blöchl, P. E. *Phys. Rev. B* **1994**, *50*, 17953.
(23) Kresse, G.; Furthmüller, J. *Phys. Rev. B* **1996**, *54*, 11169.
(24) Perdew, J. P.; Burke, K.; Ernzerhof, M. *Phys. Rev. Lett.* **1996**, *77*, 3865−3868.
(25) Kohn, W.; Sham, L. J. *Phys. Rev.* **1965**, *140*, A1133.
(26) Pandey, S.; Kumar, A.; Banik, S.; Shukla, A.; Barman, S.; Pimpale, A. *Phys. Rev. B* **2008**, *77*, 113104.
(27) Gazquez, J.; Luo, W.; Oxley, M. P.; Prange, M.; Torija, M. A.; Sharma, M.; Leighton, C.; Pantelides, S. T.; Pennycook, S. J.; Varela, M. *Nano Lett.* **2011**, *11*, 973.
(28) Kim, Y. M.; He, J.; Biegalski, M. D.; Ambaye, H.; Lauter, V.; Christen, H. M.; Pantelides, S. T.; Pennycook, S. J.; Kalinin, S. V.; Borisevich, A. Y. *Nat. Mater.* **2012**, *11*, 1−7.
(29) Stemmer, S.; Sane, A.; Browning, N. D.; Mazanec, T. J. *Solid State Ionics* **2000**, *130*, 71−80.
(30) Hansteen, O. H.; Fjellvåg, H.; Hauback, B. C. *J. Solid State Chem.* **1998**, *141*, 411−417.
(31) Hansteen, O. H.; Fjellvåg, H.; Hauback, B. C. *J. Mater. Chem.* **1998**, *8*, 2081−2088.
(32) Dachraoui, W.; Hadermann, J.; Abakumov, A. M.; Tsirlin, A. A.; Batuk, D.; Glazyrin, K.; McCammon, C.; Dubrovinsky, L.; Tendeloo, G. V. *Chem. Mater.* **2012**, *24*, 1378.
(33) Frontera, C.; García-Muñoz, J. L.; Castaño, O.; Ritter, C.; Brunelli, M. *J. Phys.: Conf. Ser.* **2010**, *200*, 012039.
(34) Klie, R. F.; Ito, Y.; Stemmer, S.; Browning, N. D. *Ultramicroscopy* **2001**, *86*, 289−302.
(35) Shimakawa, Y.; Inoue, S.; Haruta, M.; Kawai, M.; Matsumoto, K.; Sakaiguchi, A.; Ichikawa, N.; Isoda, S.; Kurata, H. *Cryst. Growth Des.* **2010**, *10*, 4713−4715.
(36) Ferguson, J. D.; Kim, Y.; Kourkoutis, L. F.; Vodnick, A.; Woll, A. R.; Muller, D. A.; Brock, J. D. *Adv. Mater.* **2011**, *23*, 1226−1230.
(37) Muller, D. A.; Nakagawa, N.; Ohtomo, A.; Grazul, J. L.; Hwang, H. Y. *Nature* **2004**, *430*, 657−661.
(38) Wang, Z. L.; Bentley, J.; Evans, N. D. *Micron* **2000**, *31*, 355−362.
(39) Riedl, T.; Gemming, T.; Wetzig, K. *Ultramicroscopy* **2006**, *106*, 284−291.
(40) Klie, R. F.; Yuan, T.; Tanase, M.; Yang, G.; Ramasse, Q. *Appl. Phys. Lett.* **2010**, *96*, 082510.
(41) Radaelli, P.; Cheong, S. W. *Phys. Rev. B* **2002**, *66*, 094408.
(42) Knížek, K.; Jirák, Z.; Hejtmánek, J.; Novák, P. *J. Phys.: Condens. Matter* **2006**, *18*, 3285.
(43) Knížek, K.; Novák, P.; Jirák, Z. *Phys. Rev. B* **2005**, *71*, 054420.
(44) Korotin, M. A.; Ezhov, S. Y.; Solovyev, I. V.; Anisimov, V. I.; Khomskii, D. I.; Sawatzky, G. A. *Phys. Rev. B* **1996**, *54*, 5309.
(45) Mizokawa, T.; Fujimori, A. *Phys. Rev. B* **1996**, *54*, 5368.
(46) The intermediate spin state can never be the ground state in an octahedral ligand field in a cubic symmetry. However, the ground state of intermediate spin configuration could be realized in certain complexes of lower symmetry than cubic.